ARTICLE

OBC
www.rsc.org/obc

Nucleophilic identity substitution reactions. The reaction between water and protonated alcohols†‡

Jon K. Laerdahl and Einar Uggerud*
Department of Chemistry, University of Oslo, PO Box 1033 Blindern, N-0315 Oslo, Norway. E-mail: einar.uggerud@kjemi.uio.no

Received 28th February 2003, Accepted 30th June 2003
First published as an Advance Article on the web 15th July 2003

The potential energy surfaces for the reaction between H_2O and the protonated alcohols $MeOH_2^+$, $EtOH_2^+$, $Pr^iOH_2^+$, and $Bu^tOH_2^+$ have been explored by means of high level *ab initio* theoretical methods. Both nucleophilic substitution (S_N2) and elimination (E2) pathways have been investigated. Front side (S_NF) and the familiar back side (S_NB) Walden inversion attack of the nucleophile have been found to be competing for the H_2O–$Bu^tOH_2^+$ system. In contradiction with the customary relationship between so-called "steric effects" and barrier heights—more alkyl-substituted S_N2 reaction centres have higher S_N2 reaction barriers—the S_N2 reaction barriers are found to be Et > Me > Pr^i > Bu^t. This result is in excellent agreement with available experimental data.

Introduction

Nucleophilic substitution reactions are among the most studied in organic chemistry, both in anionic, †‡

$$Y^- + R\text{–}X \longrightarrow Y\text{–}R + X^-, \qquad (1)$$

and in cationic form,

$$Y + R\text{–}X^+ \longrightarrow Y\text{–}R^+ + X. \qquad (2)$$

However, after nearly a century of intense research, even these classic reactions are still imperfectly understood. For these and other reactions, the rates and other kinetic parameters are usually explained in terms of potential energy diagrams or surfaces, but the properties of these surfaces—which should be viewed as theoretical constructs—are in many cases difficult to predict. While a practising chemist in many cases may derive how the physical properties of a chemical species will be modified upon some structural change, less appears to be known about how to predict changes in reactivity. A deeper insight into such fundamental concepts is among the important goals of modern physical organic chemistry.

While substitution reactions mostly are performed in solution in practical synthetic organic chemistry, it has become evident over the last decades that the complicated interactions between solute and solvent make gas phase studies a rich source of insight into reaction mechanisms and dynamical details for these reactions.[1–4] In the gas phase there are fairly strong attractive forces between the usually dipolar and charged reactants giving rise to a *double-well* potential energy diagram[5] with a reactant and a product channel ion–dipole complex which are stabilized relative to the reactants or products by $\Delta H_{\mathrm{Rcmpl}}$ and $\Delta H_{\mathrm{Pcmpl}}$, respectively. For exothermic and thermoneutral reactions, the central energy barrier between these complexes is the bottleneck for reaction once the entrance channel complex has been generated, and we denote the overall barrier (relative to reactants) $\Delta H^{\ddagger}$. More details can be found in our recent review.[1]

More than a hundred experimental studies of gas phase bimolecular substitution (S_N2) reactions—mostly mass spectrometric studies—have been performed over the last decade,[1,2,4] and it has been demonstrated that many of the properties of substitution reactions in solution that traditionally are ascribed to intrinsic properties of the reacting species, in fact are due to an interaction of intrinsic features such as substituent effects on nucleophile or substrate and the properties of the solvent. Unfortunately, it is in many cases very difficult to obtain reliable estimates of potential energy surface (PES) properties such as reaction barrier heights and overall reaction energies—exactly those parameters which chemists use to make sense of reaction rate data and to obtain chemical insight—from the gas phase experimental data. Hase and co-workers[6,7] have shown that the very simple and best studied S_N2 reactions, those between halide ions and halomethanes, do not even behave statistically and cannot be reliably interpreted applying statistical theories such as Rice–Ramsberger–Kassel–Marcus (RRKM) theory. While this behavior appears to be limited to reactions between small molecules without low frequency vibrational modes that easily may take up energy from the intermolecular relative translational energy degrees of freedom, any derived experimental reaction barrier relies heavily on theoretical input such as structural data or vibrational frequencies for critical points on the PES. Due to these difficulties, we believe that the ongoing development of accurate theoretical, in particular *ab initio*, methods and their application for understanding substitution reactions, has the potential of providing a better understanding of these reactions. A large number of theoretical publications have already appeared in the literature,[1,2] but only quite recently have the methods become of a quality capable of giving reliable quantitative predictions, for example for S_N2 reaction barriers.[8–17]

Marcus theory[4,18,19] has been applied for gas (and solution) phase S_N2 reactions and provides very important insight into the governing parameters for barrier heights of non-identity exothermic or endothermic reactions. For the elementary reaction step over the central barrier the non-identity reaction barrier is easily derived from the exothermicity of the reaction and the barrier height for the two corresponding thermoneutral identity reactions (X = Y in eqns. (1) and (2)).[4,18,20,21] For this reason, the identity reactions are of fundamental importance. Of the four common types of nucleophilic substitution reactions, only the two in eqns. (1) and (2) may be designated identity reactions.[22] Unfortunately experience and predictive tools for determining the barrier heights and reaction rates for these reactions are scarce. The only significant source of insight is through the use of valence bond (VB) correlation diagrams as

† Part I. For Part II, see following paper (DOI: 10.1039/b302270f).
‡ Electronic supplementary information (ESI) available: Cartesian coordinates for all species together with analytical imaginary frequencies for the transition structures. See http://www.rsc.org/suppdata/ob/b3/b302268d/

DOI: 10.1039/b302268d

developed by Shaik, Pross and co-workers.[4,23–26] However, as long as valence bond electron structure methods lag behind molecular orbital based methods in terms of available software tools, it might be seen as beneficial with alternative views and models of explanation.

Two important findings in the last couple of years have questioned some of the traditional views on nucleophilic substitution reactions. The first finding is concerned with the trend of increased reaction barrier height and decreased reaction rate upon increased alkyl substitution at the S_N2 reaction centre both in solution and in the gas phase. For example, for the gas phase reaction,[27,28]

$$Cl^- + R\text{–}Cl \longrightarrow Cl\text{–}R + Cl^-, \qquad (3)$$

the barrier height trend is R = Me < Et < Pr^i < Bu^t. However, Uggerud and Bache-Andreassen[29] found in 1999 that for the series of identity reactions,

$$H_2O + R\text{–}OH_2^+ \longrightarrow {}^+H_2O\text{–}R + H_2O, \qquad (4)$$

the order of the gas phase reaction rates is R = Bu^t > Pr^i > Me > Et. Theoretical calculations[29] also showed that the reaction barrier for the reaction between H_2O and $Bu^tOH_2^+$ was much lower than for the reactions with $MeOH_2^+$ and $EtOH_2^+$. *Ab initio* studies by Ruggiero and Williams subsequently confirmed these results.[28] Both the theoretical investigations of Uggerud and Bache-Andreassen[29] and of Ruggiero and Williams[28] showed a strong coupling between substituent effects—increased alkyl substitution—and solvent effects. However, while the former study[29] found a reversal to the common barrier trend R = Bu^t > Pr^i > Et > Me upon explicit addition of several water molecules in order to model solvatization, the gas phase trends were kept in the polarized continuum model calculations of Ruggiero and Williams.[28] Clearly, further investigations with more accurate theoretical models are appropriate.

Very recently Brauman and co-workers[30] showed experimentally that for the reaction of Scheme 1 with R = Me and Bu^t, the reaction barrier difference between the smallest (R = Me) and the largest (R = Bu^t) substituent is much lower in the gas phase than what one would expect from earlier studies in solution. It therefore appears that so-called steric substituent effects that commonly are viewed as purely internal of the reacting molecules actually are strongly coupled with external solvent effects in a fashion of which there currently is very little understanding.

Scheme 1

The second finding is concerned with the reaction mechanism for bimolecular S_N2 reactions that has been almost universally believed to occur *via* Walden inversion of configuration (*i.e.* reaction (I) of Scheme 2). The alternative retentitive reaction mechanism (reaction (II) of Scheme 2) has been considered as

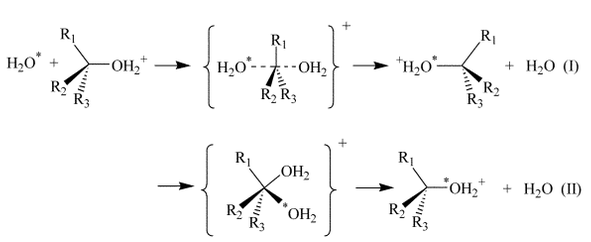

Scheme 2 Nucleophilic substitution *via* the rear-side (S_NB) and front-side (S_NF) pathway.

unimportant and with a transition state with a significantly higher energy. Actually, many organic chemists appear to have conceptual problems with a retentitive S_N2 mechanism, even though this is very common for the related system of nucleophilic attack on tetrahedral Si.[31,32] Theoretical calculations by Radom and co-workers[10] support the preferred Walden inversion pathway, with the retentitive reaction barrier lying almost 200 kJ mol^{-1} above the inversion reaction for the $CH_3Cl\text{–}Cl^-$ system. However, Uggerud and Bache-Andreassen[29] found that for the reaction (4) the retentitive front-side (S_NF) pathway is only a few kJ mol^{-1} above the Walden inversion rear-side (S_N2/S_NB) reaction for the R = Bu^t reaction. Both pathways are definitely competing in this case and despite its slightly higher energy barrier, S_NF might in this case be the most important substitution since the front-side hydrogen bonded complex at the S_NF channel entrance is much lower in energy (by 60 kJ mol^{-1}) than the shallow well for the rear-side ion–dipole complex. *Ab initio* trajectory studies are currently being pursued in order to clarify this issue. In two recent studies Uggerud[33] for the protonated *exo*-bicyclo[3.1.0]hexanol–H_2O and Sauers[34] for the protonated *exo*-norbornanol–NH_3 systems have shown that S_NF actually may be energetically favored over S_NB in special cases. It should also be mentioned that front-side nucleophilic substitution has been studied in internal nucleophilic displacements[35] and in ion pair S_N2 reactions.[36] S_NF processes have also been studied in solution,[37–42] but we believe that the interpretation and detailed determination of the reaction mechanisms for the solution phase studies are less straightforward than in the gas phase due to the complicating interactions of the solvents.

In order to gain more insight into what governs reaction barriers for identity substitution reactions, general substituent effects and the competition between S_NB and S_NF pathways we have performed high quality *ab initio* calculations for the reaction (4) between water and protonated alcohols with R = Me, Et, Pr^i and Bu^t. The calculations are of higher quality than earlier studies in the respect that they are expected to give barriers and energy differences on the PES accurate to within a few kJ mol^{-1}. These are discussed in the present publication and provide a benchmark for more approximate methods. In subsequent publications[43,44] the same theoretical methods have been employed for the reactions,

$$NH_3 + R\text{–}NH_3^+ \longrightarrow {}^+H_3N\text{–}R + NH_3, \text{ and} \qquad (5)$$

$$HF + R\text{–}FH^+ \longrightarrow {}^+HF\text{–}R + HF, \qquad (6)$$

with R = Me, Et, Pr^i, and Bu^t. Together, the reactions (4), (5) and (6) cover a broad range of nucleophilicities and substitution patterns which reveal important trends in reactivity. The competing elimination reactions (E2) have also been investigated.

Experimental

Computational details

Ab initio Hartree–Fock (HF), second order Møller–Plesset (MP2), coupled cluster singles-doubles calculations including a perturbative treatment of the triples amplitudes (CCSD(T)) and quadratic configuration interaction (QCISD(T)) calculations were performed employing the standard 6-31G(d) and 6-31G(d,p)[45,46] basis sets, as well as Dunning type cc-pV*n*Z and aug-cc-pV*n*Z[47,48] basis sets. In the current work all *ab initio* calculations where performed with the Gaussian 98 program.[49]

G2[50] and G3[51] theory are composite techniques which involve initial geometry optimizations at the HF/6-31G(d) level and subsequent calculation of zero point vibrational energies (ZPVEs) at the same level of theory. Then the geometry is reoptimized at the MP2(full)/6-31G(d) level whereupon a number

Table 1 HF, MP2, CCSD and CCSD(T) complexation energies (ΔE_{cmpl}) and overall reaction barriers ($\Delta E^{\ddagger}$) calculated with the 6-31G(d,p) basis set at geometries optimised at the MP2 level employing the 6-31G(d), 6-31G(d,p), cc-pVDZ, aug-cc-pVDZ, and cc-pVTZ basis sets. The results are for the CH_3NH_3–NH_3 system, at 0 K and excluding ZPVEs

Level of geometry optimisation	ΔE_{cmpl}/kJ mol^{-1}				$\Delta E^{\ddagger}$/kJ mol^{-1}			
	HF	MP2	CCSD	CCSD(T)	HF	MP2	CCSD	CCSD(T)
MP2/6-31G(d)	−41.16	−47.81	−46.55	−47.52	62.75	41.13	44.96	37.93
MP2(full)/6-31G(d)	−41.13	−47.81	−46.55	−47.53	62.88	41.14	44.98	37.94
MP2/6-31(d,p)	−41.08	−47.81	−46.64	−47.51	62.38	41.19	44.89	37.90
MP2/cc-pVDZ	−41.69	−47.99	−46.65	−47.55	62.14	41.08	44.97	38.04
MP2/aug-cc-pVDZ	−41.29	−47.73	−46.50	−47.44	62.30	41.15	44.85	37.82
MP2/cc-pVTZ	−41.40	−47.73	−46.51	−47.42	63.22	41.21	45.12	38.09

of single-point MP2, MP4 and QCISD(T) calculations are performed in order to obtain an energy estimate which is effectively at the QCISD(T)/G3Large and QCISD(T)/6-311+G(3df,2p) level for G3 and G2, respectively. In the present work, modified Gn schemes were employed since many of the optimized critical point structures deviate substantially in geometry on the MP2 and HF PES. For this reason, the standard G2 and G3 schemes were employed, but modified such that also the ZPVEs were calculated at the MP2/6-31G(d) level and scaled according to Scott and Radom[52] (scaling factor = 0.9434 matches 'higher level correction' of Gn theory[52]). These slightly improved Gn schemes are termed Gn_m in the present work and are expected to give results of the quality usually obtained with Gn theory for closed shell interactions without significant non-dynamical correlation effects, *i.e.* errors of not more than a few kJ mol^{-1} for reaction energies and barriers. This accuracy of the Gn methods has previously been demonstrated for S_N2 reactions.[8,9,11]

Due to the large number of low energy vibrational modes and complicated structure of the PESs, all searches for transition structures were performed with the full analytical Hessian calculated at every point in the geometry optimization procedure. No symmetry constraints were employed. All stationary points were characterized by a full analytic frequency calculation. Intrinsic reaction co-ordinate (IRC) calculations were performed for all transition structures in order to check that they were connecting the expected energy minima. The MP2/6-31G(d) ZPVEs were scaled according to Scott and Radom[52] (scaling factor = 0.967). All Gn_m and MP2 energies presented are 0 K energies including ZPVEs unless otherwise stated.

Results and discussion

One of the main ideas behind the very successful model chemistries such as G2,[50] G3,[51] and the Weizmann-theories of Martin and co-workers[53] is that the geometry optimization which involves costly calculations of energy gradients and Hessians may be performed at a fairly low level of theory such as MP2 or density functional B3LYP with a double-zeta basis set, while the single point calculations needed to finally determine energy barriers and reaction energies should be performed at a high level of theory (CCSD(T)/QCISD(T)) and with large basis sets. Table 1 is an illustration of the validity of this assumption for the type of systems we are currently investigating. Each horizontal row contains ΔE_{cmpl} and $\Delta E^{\ddagger}$ calculated in *single point* energy calculations at a geometry that has been optimized with a given basis set and method. It is easily seen that for the *geometry optimization*, including core electrons in the correlation treatment (row 2), polarization functions for the hydrogen atoms (row 3), adding diffuse functions (row 5) or switching to a triple-zeta basis set (row 6) has a negligible effect on both ΔE_{cmpl} and $\Delta E^{\ddagger}$. However, as seen from comparing the different columns of Table 1, it is highly important to use a high level of theory—*i.e.* CCSD(T) or QCISD(T)—for the *single point* energy calculations at the stationary points that are used to determine ΔE_{cmpl} and in particular $\Delta E^{\ddagger}$. Note that as seen from a comparison of rows 4 and 5 additional diffuse functions (*e.g.* as in 6-31+G(d) or aug-cc-pVXZ) are not necessary for the geometry optimizations for the current systems. This is most likely due to the cationic character of the involved species.

G2 and G3 theory are also known to have problems for calculations on systems with significant multiconfigurational character.[54,55] Calculations of the MP2 natural orbital occupation numbers[56] for the CH_3NH_3–NH_3 system—1.96/1.95 and 0.03/0.04 for the ion–dipole complex/transition state for the HOMO and LUMO, respectively—indicate that static correlation is unimportant for the systems currently under investigation. In conclusion, these systems should be well suited for the $G2_m$/$G3_m$ treatment, and we expect an accuracy of well below 10 kJ mol^{-1} for the energy barriers and energy differences on the PESs.

Optimized MP2/6-31G(d) geometries for the stationary points on the PES for the reactions (4) between H_2O and ROH_2^+ and the competing E2 reactions are given in Figs. 1–4 for R = Me, Et, Pr^i, and Bu^t. Cartesian co-ordinates for all species are given in the Supplementary material† together with analytical imaginary frequencies for the transition structures. Relative energies at the $G3_m$, $G2_m$, and MP2/6-31G(d) level are given in Figs. 5–8, where the drawn PESs correspond to $G3_m$. The vertical scale is the same in Figs. 5–8.

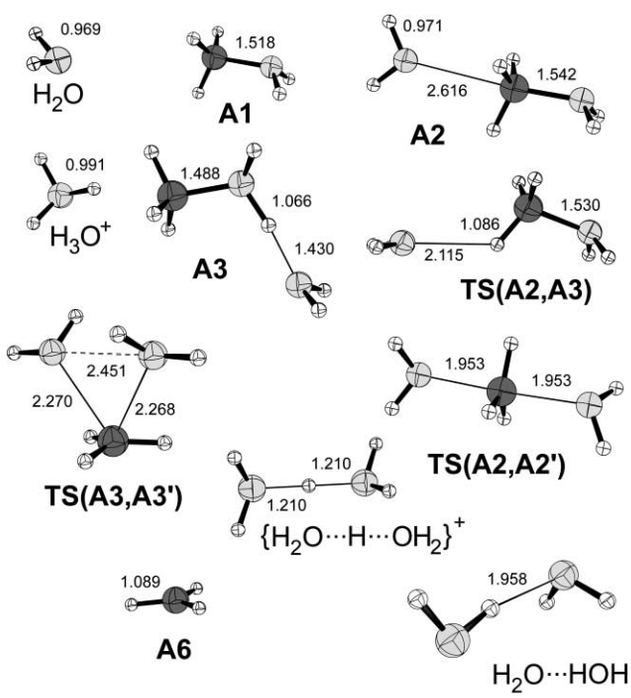

Fig. 1 Structures of stationary points on the PES for the substitution reaction between H_2O and $MeOH_2^+$ as well as H_2O, H_3O^+, their adduct, and the water dimer calculated at the MP2/6-31G(d) level. All bond lengths are given in Å. Cartesian coordinates for these structures have been included as Supplementary material.†

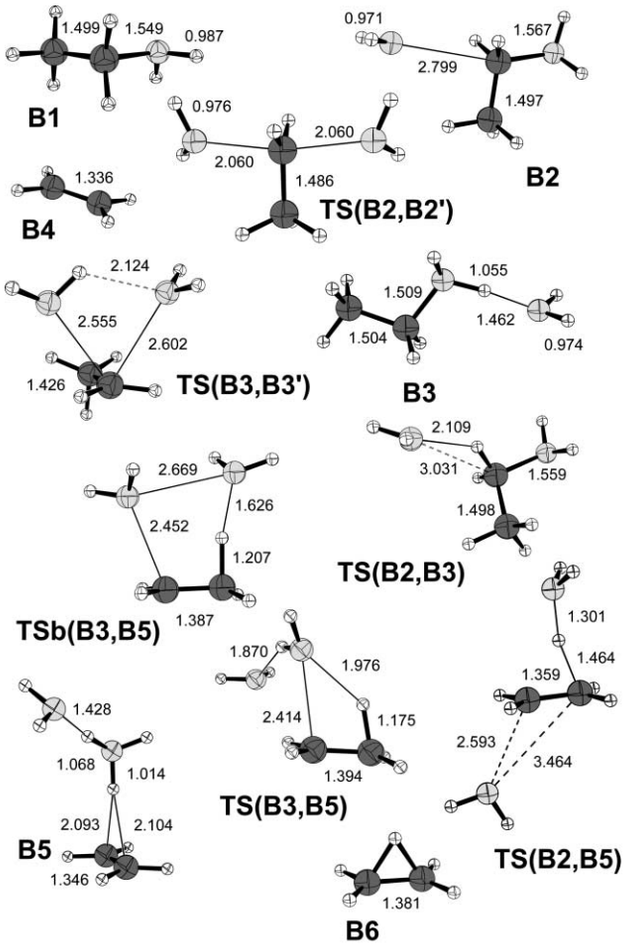

Fig. 2 Structures of stationary points on the PES for the substitution and elimination reaction between H_2O and $EtOH_2^+$ calculated at the MP2/6-31G(d) level. All bond lengths are given in Å. Cartesian coordinates for these structures have been included as Supplementary material. †

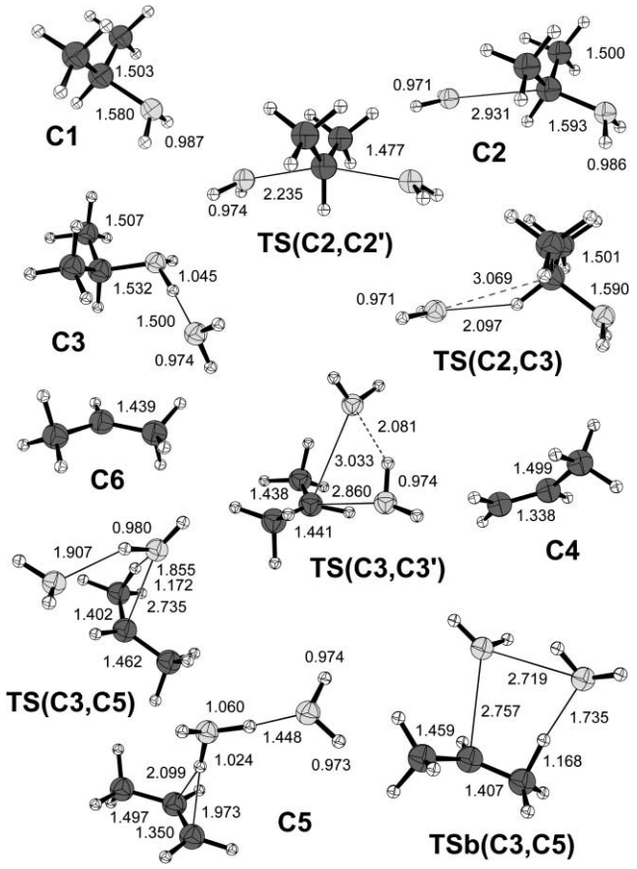

Fig. 3 Structures of stationary points on the PES for the substitution and elimination reaction between H_2O and $Pr^iOH_2^+$ calculated at the MP2/6-31G(d) level. All bond lengths are given in Å. Cartesian coordinates for these structures have been included as Supplementary material. †

The computational cost of $G3_m$ calculations is approximately half that of $G2_m$, and the accuracy is expected to be similar for the two theories.[51] Indeed, for the substitution pathways, the $G2_m$ and $G3_m$ results agree perfectly, with differences of the order of 1–2 kJ mol^{-1} and none larger than 3.3 kJ mol^{-1}. The less accurate MP2/6-31G(d) method invariably overestimates the stabilization of the complexes relative to $G2_m$/$G3_m$, by approximately 20 and 10 kJ mol^{-1} for the front and rear side complexes, respectively. The MP2 barrier $\Delta H^{\ddagger}$ also deviates from the $G2_m$/$G3_m$ result, by between 5 and 10 kJ mol^{-1}, but there is no systematic over- or underestimation. For the E2 pathway there are slightly larger differences between the $G2_m$ and $G3_m$ results (but still < 5 kJ mol^{-1}), and the MP2 results do not deviate significantly in this case.

It should be noted that while the PES of the H_2O–$MeOH_2^+$ system is fairly uncomplicated, the larger systems have a large number of local energy minima and many competing pathways for reactions with transition state barriers that only differ by a few or only a fraction of a kJ mol^{-1}. As an example, there are within an interval of 2.3 kJ mol^{-1} four different transition structures for the elimination **TS(C3,C5)** which only differ by the angle and dihedral angle between the $(H_2O)_2$ and $CH_3CHCH_3^+$ moieties. In addition there is the competing **TSb(C3,C5)** pathway with a transition state a few kJ mol^{-1} higher in energy. The structures of Figs. 1–4 all correspond to the lowest energy minima and pathways that were detected. The very complicated structure of the PESs and the large number of competing pathways of similar energy have two important consequences. It should be noted that these are of relevance for all studies of organic chemical systems of a complexity similar to or higher than the species involved in the current study. Firstly, only very reliable and well tested theoretical algorithms are capable of finding all relevant critical points on the PESs and a very significant amount of manual work is needed to locate (or make probable the non-existence) of these transition structures or energy minima. Secondly, traditional statistical theories such as RRKM most likely are going to struggle to reliably predict reaction rates and in particular branching rates between competing reaction pathways. A possible partial solution to these problems is the introduction of reliable *ab initio* molecular dynamics algorithms which makes it possible to follow a large number of trajectories on reliable PESs.[57]

There are no large geometry changes for the protonated alcohol moieties going from the reactants **X1** (**X** = **A**, **B**, **C**, and **D**) to the front side (**X3**) and rear side (**X2**) complexes. In all four systems the front side hydrogen bonded complexes **X3** are the global energy minima with the rear side ion–dipole complexes **X2** at least 50 kJ mol^{-1} higher in energy. The rear side energy well on the PES is shallow for H_2O–$MeOH_2^+$ while disappearing almost completely for H_2O–$EtOH_2^+$ and H_2O–$Pr^iOH_2^+$. It is also quite shallow for H_2O–$Bu^tOH_2^+$ where the water molecule must travel a significant distance to move from rear to front side position *via* **TS(D2,D3)**. In agreement with the Leffler–Hammond assumption, the transition state for the transfer of H_2O from the rear to front side position is very early—as measured by the difference of the O–C_1–O angle in the back side complex **X2** and in the transition structure **TS(X2,X3)** (**X** = **A**, **B**, and **C**)—for these systems and the earliest for the reactions with the lowest barriers.

The Walden inversion transition structures **TS(X2,X2′)** are characterized by a significant extension of the C_1–O bond that is being broken compared with the rear side complexes **X2**. The

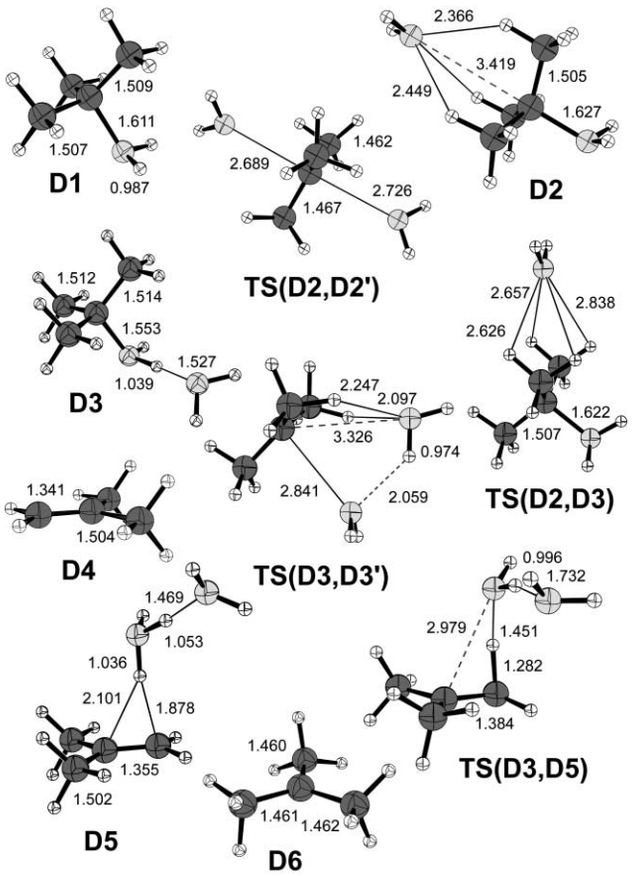

Fig. 4 Structures of stationary points on the PES for the substitution and elimination reaction between H_2O and $Bu^tOH_2^+$ calculated at the MP2/6-31G(d) level. All bond lengths are given in Å. Cartesian coordinates for these structures have been included as Supplementary material. †

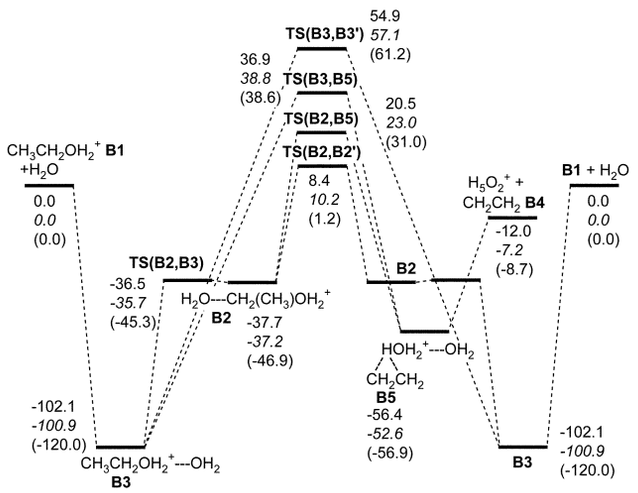

Fig. 6 Potential energy diagram for the substitution and elimination reaction between H_2O and $EtOH_2^+$ calculated at the $G3_m$ level. The calculated energies at the $G2_m$ and MP2/6-31G(d) (including ZPVE corrections) level are given in italics and in parentheses, respectively. All relative energies are given in kJ mol^{-1} at 0 K.

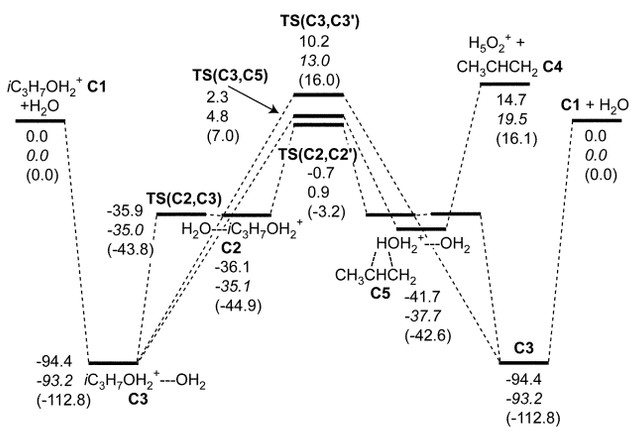

Fig. 7 Potential energy diagram for the substitution and elimination reaction between H_2O and $Pr^iOH_2^+$ calculated at the $G3_m$ level. The calculated energies at the $G2_m$ and MP2/6-31G(d) (including ZPVE corrections) level are given in italics and in parentheses, respectively. All relative energies are given in kJ mol^{-1} at 0 K.

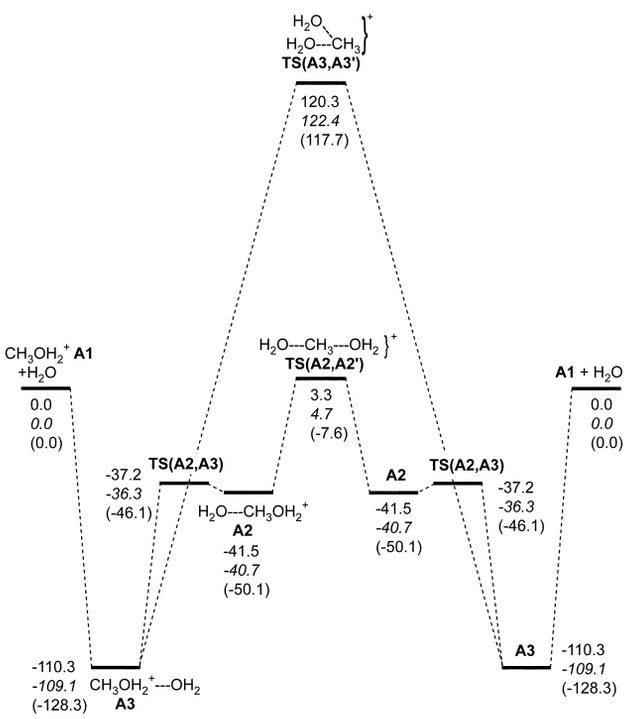

Fig. 5 Potential energy diagram for the substitution reaction between H_2O and $MeOH_2^+$ calculated at the $G3_m$ level. The calculated energies at the $G2_m$ and MP2/6-31G(d) (including ZPVE corrections) level are given in italics and in parentheses, respectively. All relative energies are given in kJ mol^{-1} at 0 K.

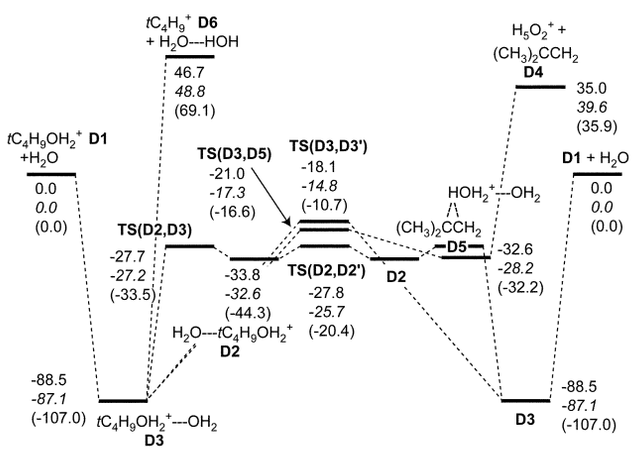

Fig. 8 Potential energy diagram for the substitution and elimination reaction between H_2O and $Bu^tOH_2^+$ calculated at the $G3_m$ level. The calculated energies at the $G2_m$ and MP2/6-31G(d) (including ZPVE corrections) level are given in italics and in parentheses, respectively. All relative energies are given in kJ mol^{-1} at 0 K.

bond elongation is 0.44, 0.49, 0.64 and 1.1 Å for R = Me, Et, Pr^i and Bu^t, respectively. The corresponding shortening of the C_1–O bond that is being formed is rather similar for the four systems at 0.66, 0.74, 0.70, and 0.73 Å. As discussed earlier by Ruggiero and Williams[28] and by Uggerud and Bache-Andreassen[29] there are three transition states, corresponding to rotations of the three methyl groups, in the transition state region for the Walden inversion of the H_2O–$Bu^tOH_2^+$ system. **TS(D2,D2′)** is the highest and central barrier and is flanked by two symmetric shallow intermediates and transition states that are 3.9 and 3.8 kJ mol^{-1} below **TS(D2,D2′)**, respectively, at the MP2/6-31G(d) level. Cartesian co-ordinates for these intermediates and transition structures are given in the Supplementary material.† It is not likely, however, that this feature is of great dynamical importance, since upon addition of ZPVEs the energies for the two symmetric intermediates and transition structures become identical at 2.8 kJ mol^{-1} below **TS(D2,D2′)**. At the $G3_m$ ($G2_m$) level the intermediates and TSs are only 1.0 (0.8) and 0.3 (0.1) kJ mol^{-1} below **TS(D2,D2′)**. All the rear side transition structures **TS(X2,X2′)** (**X** = **A**, **B**, **C**, and **D**) are below (Bu^t), at the same level (Pr^i) or slightly above the energy of the reactants (Me and Et). This agrees well with the experimental findings since all substitutions were observed in the gas phase by Uggerud and Bache-Andreassen.[29] Note that thermoneutral nucleophilic substitution reactions in most cases do not occur at detectable rates since their barriers are significantly higher than the energy of the reactants.[1]

The front side substitution transition structures **TS(X3,X3′)** (**X** = **A**, **B**, and **C**) all have C_1–O distances that are significantly longer, by between 0.3 and 0.6 Å, than in the corresponding Walden inversions. The front side reaction barriers of **TS(X3,X3′)** are also much higher in energy than **TS(X2,X2′)** for the H_2O–ROH_2^+ (R = Me and Et) systems and the front side substitution is not expected to compete with Walden inversion except at very high energies. On the other hand, the front side substitution **TS(D3,D3′)** for R = Bu^t is only 10 kJ mol^{-1} (Gn_m level) above Walden inversion **TS(D2,D2′)** and of the order of 15–20 kJ mol^{-1} below the energy of the reactants. In this case, it is obvious that substitution *via* the front or back side pathway is determined solely by the dynamics and front side nucleophilic substitution may occur at least as frequently as Walden inversion. The reaction system may be viewed as a Bu^{t+} carbocation solvated by two water molecules. The R = Pr^i system is in an intermediate region with the front side **TS(C3,C3′)** being approximately 10 kJ mol^{-1} above both the reactant and the Walden inversion **TS(C2,C2′)** energies. In this case it is not obvious to what degree front side substitution will occur, and further dynamical studies are in order to investigate this issue further.

The order of reaction rates for the reactions (4) determined by Uggerud and Bache-Andreassen[29] was (from slowest to fastest): Et < Me < Pr^i < Bu^t. The reaction rate of H_2O–$Bu^tOH_2^+$ is close to the encounter rate. The derived order of RRKM reaction barriers[29] was Et > Me > Pr^i > Bu^t. The order of Walden inversion substitution reaction barriers was however calculated to be Et > Pr^i > Me > Bu^t at the B3LYP and MP2 level,[29] the MP2 results being nearly identical to the MP2 values of Figs. 5–8. Our new $G3_m$ (and $G2_m$) refined results of Figs. 5–8 now have the order of barrier heights (in kJ mol^{-1})—$\Delta H^{\ddagger}$(Et) = 8.4 > $\Delta H^{\ddagger}$(Me) = 3.3 > $\Delta H^{\ddagger}$(Pr^i) = −0.7 > $\Delta H^{\ddagger}$(Bu^t) = −27.8—in perfect agreement with the experimental reaction rates and RRKM barriers. The very low barrier for R = Bu^t agrees with the finding that for this reaction the rate is close to the gas phase encounter rate.

The PESs for the elimination reactions,

$$H_2O + CH_3CR_1R_2–OH_2^+ \longrightarrow CH_2CR_1R_2 + H_5O_2^+, \quad (7)$$

(R_1, R_2 = H, CH_3) are also given in Figs. 6–8. The reaction intermediates **X5** (**X** = **B**, **C**, and **D**) are all significantly lower in energy than the reactants. We expected the transition structures **TS(X3,X5)** where the two water molecules "co-operate" in removing the proton from the alkyl moiety to correspond to the lowest energy elimination pathway, but this turned out not to be the case for **X** = **B** (*vide infra*). The reaction between H_2O and $EtOH_2^+$ is exothermic, but the energy of the transition structures **TS(B3,B5)** and **TS(B2,B5)** is fairly high, and no E2 reaction was observed by Uggerud and Bache-Andreassen.[29] The elimination reactions of H_2O–$Pr^iOH_2^+$ and H_2O–$Bu^tOH_2^+$ have lower barriers, but the formation of $H_5O_2^+$ and the alkenes **X4** (**X** = **C** and **D**) is endothermic. They were still observed in room temperature experiments, and possible explanations for this observation have been discussed elsewhere.[29]

The calculated $G3_m$ 0 K proton affinity for the water dimer is 809 kJ mol^{-1}. The experimental values[58,59] ($G3_m$ results) are 691 (683), 681 (671), 752 (739) and 802 (798) kJ mol^{-1}, for water, ethylene, propylene, and *iso*-butylene, respectively. Consequently, the water dimer may easily abstract a proton from all three protonated alkenes, whereas the single water molecule only will do this from protonated ethylene itself. The transition structures **TSb(X3,X5)** (**X** = **B** and **C**) of Figs. 2 and 3 represent alternative elimination pathways, where a single water molecule picks off the proton while at the same time the remaining moiety is stabilized by the other water molecule. The two transition states lie only 0.3 and 6.6 kJ mol^{-1} above the alternative **TS(X3,X5)** pathways in energy for the Et and Pr^i systems, respectively. These two possible elimination pathways are definitely competing for these molecules. Despite a number of attempts we were unable to locate a similar **TSb** type transition structure for the Bu^t system, most likely due to the higher proton affinity of *iso*-butylene. A third elimination pathway was found for the H_2O–$EtOH_2^+$ system, **TS(B2,B5)**, in which the 'spectator' water molecule is on the rear side of the Et moiety. This is the lowest elimination pathway of Fig. 6. We were not able to locate similar transition structures for the Pr^i and Bu^t systems, undoubtedly connected with the higher proton affinities of propylene and *iso*-butylene. In order to investigate this further, we calculated the PESs for the elimination of H_3O^+ from ROH_2^+ (R = Et, Pr^i, and Bu^t) given in Fig. 9. The figure illustrates how the increased difference in proton affinity between water and the ethylene derivatives gives for the reverse reaction a transition from a significant energy barrier for $EtOH_2^+$, a tiny (negative upon addition of the ZPVE) barrier for $Pr^iOH_2^+$ and no barrier for $Bu^tOH_2^+$. For the reaction (7) where two water molecules may co-operate in the elimination reaction, the **TS(B2,B5)** reaction barrier is the lowest for H_2O–$EtOH_2^+$, most likely due to efficient stabilization and weakening of the C–O bond being broken by the rear side water molecule. At the other extreme, the Bu^{t+} moiety of Fig. 4 may only be deprotonated by the water *dimer* and no transition structure of the **TS(X2,X5)** or **TSb(X3,X5)** type exists. An alternative reaction pathway illustrated in Fig. 8 gives the carbocation (**D6**) and the water dimer. However, this reaction is relatively endothermic, and even more so for the H_2O–$EtOH_2^+$ and H_2O–$Pr^iOH_2^+$ systems—by 126.7 and 85.1 kJ mol^{-1} at the $G3_m$ level, respectively.

The 'hidden' pathway for front side substitution that previously has been discussed by Uggerud and Bache-Andreassen[29] involves a passage over the **TS(X3,X5)** transition barrier, an exchange of the two water molecules, *i.e.* a **TS(X5,X5′)** and passage back over the elimination transition barrier **TS(X5′,X3′)**. While this is lower in energy than the direct **TS(X3,X3′)** pathway, it is perhaps not of importance in practice, since dynamically the system will most likely not be trapped in the fairly shallow post reaction complex **X5** energy well. The absence of such trapping and corresponding lack of intramolecular vibrational energy redistribution have recently been discussed by Hase and co-workers.[7]

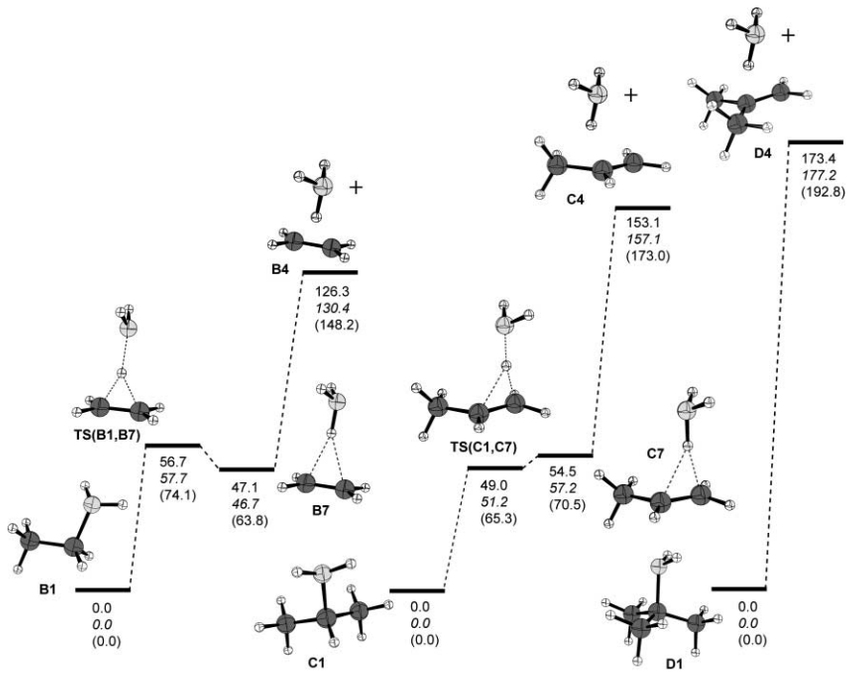

Fig. 9 Potential energy diagrams for elimination of H_3O^+ from ROH_2^+ (R = Et, Pr^i, and Bu^t) calculated at the $G3_m$ level. The calculated energies at the $G2_m$ and MP2/6-31G(d) (including ZPVE corrections) level are given in italics and in parentheses, respectively. All relative energies are given in kJ mol^{-1} at 0 K.

Conclusion

Ab initio quantum chemistry has recently reached a level of precision where reaction energies and barriers can be calculated with high accuracy—well below 10 kJ mol^{-1}—for closed shell systems without complicating issues such as near-degeneracies and instabilities. In many cases these energy parameters can be derived from *ab initio* theory for systems involving organic species with less than 8–10 non-hydrogen atoms with higher confidence and with fewer assumptions than from experiment. In the current study such high level methods have been applied for the study of identity S_N2 as well as E2 reactions involving reaction systems (H_2O–Alkyl-OH_2^+) that currently are of significant interest since their properties contradict several established truths about how organic reactions occur. The same methods have also been employed to study related systems,[43,44] and it is hoped that together with the current study the theoretical data will contribute to a better understanding of several aspects of organic reactivity.

Acknowledgements

The authors wish to thank NFR (The Norwegian Research Council) for financial support through a postdoctoral fellowship for JKL. We are also grateful for a generous grant of computing time from NOTUR (The Norwegian High Performance Computing Consortium).

References

1 J. K. Laerdahl and E. Uggerud, *Int. J. Mass Spectrom.*, 2002, **214**, 277.
2 S. Gronert, *Chem. Rev.*, 2001, **101**, 329.
3 C. H. DePuy, *J. Org. Chem.*, 2002, **67**, 2393.
4 S. S. Shaik, H. B. Schlegel and S. Wolfe, *Theoretical Aspects of Physical Organic Chemistry: The S_N2 Reaction*, John Wiley, New York, 1992.
5 W. N. Olmstead and J. I. Brauman, *J. Am. Chem. Soc.*, 1977, **99**, 4219.
6 W. L. Hase, *Science*, 1994, **266**, 998.
7 L. Sun, K. Song and W. L. Hase, *Science*, 2002, **296**, 875.
8 M. N. Glukhovtsev, A. Pross and L. Radom, *J. Am. Chem. Soc.*, 1995, **117**, 2024.
9 M. N. Glukhovtsev, A. Pross and L. Radom, *J. Am. Chem. Soc.*, 1996, **118**, 6273.
10 M. N. Glukhovtsev, A. Pross, H. B. Schlegel, R. D. Bach and L. Radom, *J. Am. Chem. Soc.*, 1996, **118**, 11258.
11 S. Parthiban, G. de Oliveira and J. M. L. Martin, *J. Phys. Chem. A*, 2001, **105**, 895.
12 S. Hoz, H. Basch, J. L. Wolk, T. Hoz and E. Rozental, *J. Am. Chem. Soc.*, 1999, **121**, 7724.
13 P. Botschwina, M. Horn, S. Seeger and R. Oswald, *Ber. Bunsenges. Phys. Chem.*, 1997, **101**, 387.
14 P. Botschwina, *Theor. Chem. Acc.*, 1998, **99**, 426.
15 S. Schmatz, P. Botschwina and H. Stoll, *Int. J. Mass Spectrom.*, 2000, **201**, 277.
16 S. Schmatz, *Chem. Phys. Lett.*, 2000, **330**, 188.
17 I. Lee, C. K. Kim, C. K. Sohn, H. G. Li and H. W. Lee, *J. Phys. Chem. A*, 2002, **106**, 1081.
18 M. L. Chabinyc, S. L. Craig, C. K. Regan and J. I. Brauman, *Science*, 1998, **279**, 1882.
19 R. A. Marcus, *Annu. Rev. Phys. Chem.*, 1964, **15**, 155.
20 M. J. Pellerite and J. I. Brauman, *J. Am. Chem. Soc.*, 1980, **102**, 5993.
21 M. J. Pellerite and J. I. Brauman, *J. Am. Chem. Soc.*, 1983, **105**, 2672.
22 T. H. Lowry and K. S. Richardson, *Mechanism and Theory in Organic Chemistry*, Harper & Row, New York, 1981.
23 S. Shaik, *Isr. J. Chem.*, 1985, **26**, 367.
24 S. Shaik, *Acta Chem. Scand.*, 1990, **44**, 205.
25 S. Shaik, *Valence bond curve crossing models*, in *Encyclopedia of computational chemistry*, P. v. R. Schleyer (Ed.), John Wiley, Chichester, UK, 1998, Vol. 5, p. 3143.
26 S. Shaik and A. Shurki, *Angew. Chem., Int. Ed.*, 1999, **38**, 586.
27 F. Jensen, *Chem. Phys. Lett.*, 1992, **196**, 368.
28 G. D. Ruggiero and I. H. Williams, *J. Chem. Soc., Perkin Trans. 2*, 2001, 448.
29 E. Uggerud and L. Bache-Andreassen, *Chem. Eur. J.*, 1999, **5**, 1917.
30 C. K. Regan, S. L. Craig and J. I. Brauman, *Science*, 2002, **295**, 2245.
31 A. R. Bassindale and P. G. Taylor, *Reaction mechanisms of nucleophilic attack at silicon*, in *The Chemistry of Organic Silicon Compounds*, S. Patai and Z. Rappoport (Eds.), Wiley, Chichester, 1989, p. 839.
32 R. J. P. Corriu and J. C. Young, *Hypervalent silicon compounds*, in *The Chemistry of Organic Silicon Compounds*, S. Patai and Z. Rappoport (Eds.), Wiley, Chichester, 1989, p. 1241.
33 E. Uggerud, *J. Org. Chem.*, 2001, **66**, 7084.
34 R. R. Sauers, *J. Org. Chem.*, 2002, **67**, 1221.
35 P. R. Schreiner, P. v. R. Schleyer and R. K. Hill, *J. Org. Chem.*, 1994, **59**, 1849.
36 S. Harder, A. Streitwieser, J. T. Petty and P. v. R. Schleyer, *J. Am. Chem. Soc.*, 1995, **117**, 3253.
37 K. Okamoto, K. Takeuchi and T. Inoue, *J. Chem. Soc., Perkin Trans. 2*, 1980, 842.

38 N. T. Anh and C. Minot, *J. Am. Chem. Soc.*, 1980, **102**, 103.
39 D. E. Sunko, H. Vancik, V. Deljac and M. Milun, *J. Am. Chem. Soc.*, 1983, **105**, 5364.
40 P. E. Dietze and M. Wojciechowski, *J. Am. Chem. Soc.*, 1990, **112**, 5240.
41 F. M. Bickelhaupt, *J. Comput. Chem.*, 1999, **20**, 114.
42 I. H. Williams, *Concerted Organic and Bio-organic mechanism*, CRC Press, Boca Raton, 2000.
43 J. K. Laerdahl, L. Bache-Andreassen and E. Uggerud, *Org. Biomol. Chem.*, 2003, DOI: 10.1039/b302270f.
44 P. U. Civcir, L. Bache-Andreassen, J. K. Laerdahl, K. Faegri, Jr. and E. Uggerud, manuscript in preparation.
45 W. J. Hehre, R. Ditchfield and J. A. Pople, *J. Chem. Phys.*, 1972, **56**, 2257.
46 P. C. Hariharan and J. A. Pople, *Theor. Chim. Acta*, 1973, **28**, 213.
47 T. H. Dunning, Jr., *J. Chem. Phys.*, 1989, **90**, 1007.
48 D. E. Woon and T. H. Dunning, Jr., *J. Chem. Phys.*, 1993, **98**, 1358.
49 M. J. Frisch, G. W. Trucks, H. B. Schlegel, G. E. Scuseria, M. A. Robb, J. R. Cheeseman, V. G. Zakrzewski, J. A. Montgomery, Jr., R. E. Stratmann, J. C. Burant, S. Dapprich, J. M. Millam, A. D. Daniels, K. N. Kudin, M. C. Strain, O. Farkas, J. Tomasi, V. Barone, M. Cossi, R. Cammi, B. Mennucci, C. Pomelli, C. Adamo, S. Clifford, J. Ochterski, G. A. Petersson, P. Y. Ayala, Q. Cui, K. Morokuma, P. Salvador, J. J. Dannenberg, D. K. Malick, A. D. Rabuck, K. Raghavachari, J. B. Foresman, J. Cioslowski, J. V. Ortiz, A. G. Baboul, B. B. Stefanov, G. Liu, A. Liashenko, P. Piskorz, I. Komaromi, R. Gomperts, R. L. Martin, D. J. Fox, T. Keith, M. A. Al-Laham, C. Y. Peng, A. Nanayakkara, M. Challacombe, P. M. W. Gill, B. G. Johnson, W. Chen, M. W. Wong, J. L. Andres, C. Gonzales, M. Head-Gordon, E. S. Replogle and J. A. Pople. Gaussian 98 (Revision A.11); Gaussian, Inc.: Pittsburgh, PA, 2001.
50 L. A. Curtiss, K. Raghavachari, G. W. Trucks and J. A. Pople, *J. Chem. Phys.*, 1991, **94**, 7221.
51 L. A. Curtiss, K. Raghavachari, P. C. Redfern, V. Rassolov and J. A. Pople, *J. Chem. Phys.*, 1998, **109**, 7764.
52 A. P. Scott and L. Radom, *J. Phys. Chem.*, 1996, **100**, 16502.
53 J. M. L. Martin and G. de Oliveira, *J. Chem. Phys.*, 1999, **111**, 1843.
54 T. I. Sølling, D. M. Smith, L. Radom, M. A. Freitag and M. S. Gordon, *J. Chem. Phys.*, 2001, **115**, 8758.
55 B. K. Carpenter, *J. Phys. Chem. A*, 2001, **105**, 4585.
56 T. Helgaker, P. Jørgensen and J. Olsen, *Molecular electronic-structure theory*, Wiley, Chichester, UK, 2000.
57 K. Bolton, W. L. Hase and G. H. Peshlherbe, in *Modern Methods for Multidimensional Dynamics Computations in Chemistry*, D. L. Thompson (Ed.), World Scientific, Singapore, 1998.
58 E. P. Hunter and S. G. Lias, *J. Phys. Chem. Ref. Data*, 1998, **27**, 413.
59 P. J. Linstrom and W. G. Mallard (Eds.), *NIST Chemistry WebBook, NIST Standard Reference Database Number 69*, National Institute of Standards and Technology, Gaithersburg MD, 20899 (http: //webbook.nist.gov), 2001.